θ方向に回転する(外壁が$-W_m$で移動し，$-\Omega$で回転する)円柱座標系(r, θ, z)をとった．マシンの推進により，マシン近傍に速度勾配の大きい領域ができる．この領域を境界層といい，この領域の外側の流体はマシンの泳動による影響を受けない．これまでの2次元解析では，解析モデルのマシン長さを無限長としたため，この境界層の表現が不可能であった．従って，境界層厚さに相当する位置R_2に外壁を設け，R_2をフィッティングパラメータとし実験を参考に決定した．これに対し，3次元解析では，マシンの長さは有限長とし，計算領域はマシン周辺である．マシンの端面の流体から受ける影響については，正確に計算でき，境界層についても表現できるので，フィッティングパラメータは必要としない．

2.3 基礎方程式

前節より円柱座標系(r, θ, z)に対して，z方向にW_mで移動し，θ方向にΩで回転する座標系(r, θ', z')を用いる．対応する速度成分を(u, v', w')とおくと，

$$\begin{cases} \theta = \theta' + \Omega t \\ z = z' + W_m t \end{cases} \tag{1}$$

$$\begin{cases} v = v' + \Omega r \\ w = w' + W_m \end{cases} \tag{2}$$

となる．(1)，(2)式より，定常問題でのナビエ・ストークス方程式は，以下のようになる[3]．

$$u\frac{\partial u}{\partial r} + \frac{v'}{r}\frac{\partial u}{\partial \theta'} + w'\frac{\partial u}{\partial z'} + W_m\frac{\partial u}{\partial z'} - \frac{v'^2}{r} - 2\Omega v' - r\Omega^2 = -\frac{\partial p}{\partial r} + \frac{1}{Re}\left(\frac{\partial^2 u}{\partial r^2} + \frac{1}{r}\frac{\partial u}{\partial r} - \frac{u}{r^2} + \frac{1}{r^2}\frac{\partial^2 u}{\partial \theta'^2} - \frac{2}{r^2}\frac{\partial v'}{\partial \theta'} + \frac{\partial^2 u}{\partial z'^2}\right) \tag{3}$$

$$u\frac{\partial v'}{\partial r} + \frac{v'}{r}\frac{\partial v'}{\partial \theta'} + w'\frac{\partial v'}{\partial z'} + W_m\frac{\partial v'}{\partial z'} + \frac{uv'}{r} + 2\Omega u = -\frac{1}{r}\frac{\partial p}{\partial \theta'} + \frac{1}{Re}\left(\frac{\partial^2 v'}{\partial r^2} + \frac{1}{r}\frac{\partial v'}{\partial r} - \frac{v'}{r^2} + \frac{1}{r^2}\frac{\partial^2 v'}{\partial \theta'^2} + \frac{2}{r^2}\frac{\partial u}{\partial \theta'} + \frac{\partial^2 v'}{\partial z'^2}\right) \tag{4}$$

$$u\frac{\partial w'}{\partial r} + \frac{v'}{r}\frac{\partial w'}{\partial \theta'} + w'\frac{\partial w'}{\partial z'} + W_m\frac{\partial w'}{\partial z'} = -\frac{\partial p}{\partial z'} + \frac{1}{Re}\left(\frac{\partial^2 w'}{\partial r^2} + \frac{1}{r}\frac{\partial w'}{\partial r} + \frac{1}{r^2}\frac{\partial^2 w'}{\partial \theta'^2} + \frac{\partial^2 w'}{\partial z'^2}\right) \tag{5}$$

(3)－(5)式中のReはレイノルズ数であり次式で表される．

$$Re = \frac{\tilde{\Omega}\tilde{R}_1^2}{\tilde{\nu}} \tag{6}$$

ここで，$\tilde{\nu}$は動粘度，$\tilde{R}_1$はマシンの胴体半径である．
連続の式は(7)式で表される．

$$\frac{\partial u}{\partial r} + \frac{u}{r} + \frac{1}{r}\frac{\partial v'}{\partial \theta'} + \frac{\partial w'}{\partial z'} = 0 \tag{7}$$

以上の基礎方程式は，無次元量で表されており，速度，長さ，圧力の代表量はそれぞれ，$\tilde{\Omega}\tilde{R}_1$，$\tilde{R}_1$，$\rho(\tilde{\Omega}\tilde{R}_1)^2$である．

次に境界条件であるが，外壁，マシン表面でのすべりなし条件から以下のように表される．

$$\begin{cases} u(R_2, \theta, z) = 0 \\ v'(R_2, \theta, z) = -\Omega R_2 \\ w'(R_2, \theta, z) = -W_m \end{cases} \tag{8}$$

$$\begin{cases} u = 0 \\ v' = 0 \\ w' = 0 \end{cases} \tag{9}$$

静止座標系からみると，十分上流側の流体はマシンの影響を受けず静止していると考えられる．この条件を回転座標系(マシンに固定され，z軸周りに回転し，軸方向に移動する座標系)からみると，上流側の流体は軸方向に一様流な速度を持ち，剛体とともに回転するため，

$$\begin{cases} u = 0 \\ v' = -\Omega r \\ w' = -W_m \end{cases} \tag{10}$$

と表される．また，下流の境界条件は，自由に流れるとし次式のように定義した．

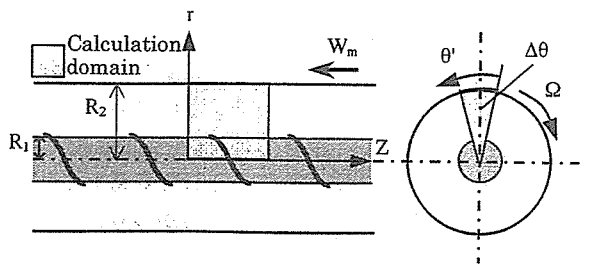

Fig. 2 Simplified model used in the two-dimensional analysis.

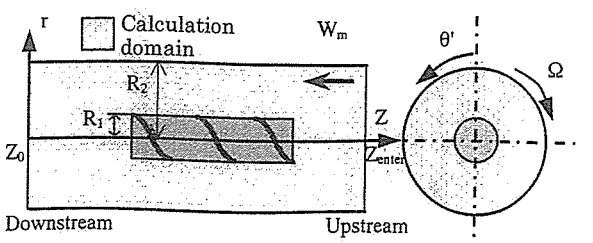

Fig. 3 Simplified model used in the three-dimensional analysis.

$$\begin{cases} \dfrac{\partial u}{\partial z'} = 0 \\ \dfrac{\partial v'}{\partial z'} = 0 \\ \dfrac{\partial w'}{\partial z'} = 0 \end{cases} \qquad (11)$$

z 軸上の特異点は参考文献[4]により決めた.

2.4 数値計算方法

流体力学の基礎方程式である，ナビエ-ストークス方程式と運動量保存の法則をスタガード格子系を用いて有限体積法で離散化し，その離散式を SIMPLER 法に類似の手法[5]で解いた．この手法は，ナビエ-ストークス方程式の対流項を QUICK スキームにより離散化することが特徴である[6]．解析には，東北大学流体科学研究所のスーパーコンピュータ Origin 2000 の 4 CPUs を用いて並列計算を行った．解析モデルの格子数は約 59 万，計算に要した CPU 経過時間は約 160 時間である．3 次元解析では，2 次元解析と比較して流れ場の値が収束しにくいため，収束計算回数を増やし，収束条件を緩めることで，流れ場の値を求めた．

上記の手法により，Fig. 4 に示すようなマシン周辺の流体の速度，圧力分布が得られる．図中の濃淡が圧力分布，矢印が速度ベクトルを表している．斜線で示しているのがマイクロマシンである．この図より，マシン推進方向を前とすると，ブレード前方と後方では後方の圧力が高い．このことから，マシンが回転することで生ずるブレード前後の流体の圧力差が推進力になっていることがわかる．回転方向のブレード前後の圧力差より，負荷トルクを求めた．速度分布からマシン表面のせん断応力に起因する負荷トルク，抗力を求める．さらに，2 次元解析では正確に計算できなかったマシン端面の影響については，圧力分布から，マシンの先端と後端の圧力差によって発生する力を抗力，速度分布から，せん断応力によりマシンの端面に発生するトルクを負荷トルクとして計算した．以上より推進方向成分として推力と抗力，回転方向成分として負荷トルクを求める．マシンの泳動速度は，推力と抗力がつりあうときの速度 W_m とした．

周波数を高くしていくとマシンが流体から受ける負荷トルクは磁気トルクを上回り，マシンは回転の同期から外れる．このときの周波数を脱調周波数と呼ぶ．この脱調周波数は回転方向成分の負荷トルクの解析結果を用いて求められる．脱調後のマシンの泳動は，脱調を繰り返しながら推進している様子を実験から確認している．脱調周波数以降は，マシンの平均回転周波数は外部からの回転磁界の周波数より小さくなる．このときのマシンの平均周波数は，マシン回転方向の運動方程式である(12)式で表される．

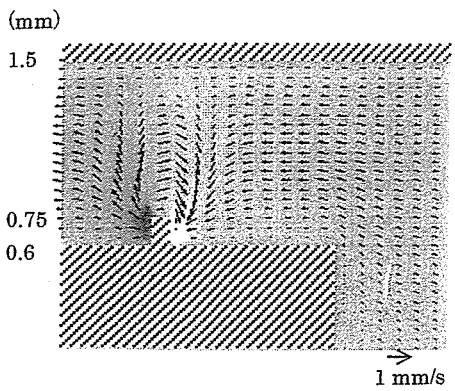

Fig. 4 Visualization of the solved flow field.

$$MH\sin(\omega t - \theta) = J\frac{d^2\theta}{dt^2} + D_f\frac{d\theta}{dt} \qquad (12)$$

M：磁石の磁気モーメント
H：外部磁界強度
ω：外部回転磁界角周波数
θ：マシン回転角
J：慣性モーメント
D_f：負荷トルクと回転速度の関係を表す比例定数

この式をルンゲ・クッタ法を用いて解き，脱調周波数以上の周波数における泳動特性を求めた[7]．

(12)式の左辺は磁気トルク，右辺第 1 項は慣性力，右辺第 2 項は流体から受ける負荷トルクを表している．負荷トルクと回転速度の関係を表す比例定数 D_f は，負荷トルクと周波数の関係の解析結果より求めた．求めた数脱調周波数以降のマシンの泳動速度はマシンの平均回転周波数での泳動速度とした．

2.5 解析結果

A. Type A

解析と実験には動粘度 1×10^5 mm²/s の液体を用いた．Fig. 5 に周波数に対する泳動速度の解析結果を示す．図中のプロットは，実験結果であり[2]，実線は 3 次元解析の結果である．図中の矢印は，実験における脱調周波数を示し 1.3 Hz であった．脱調周波数前後において，3 次元解析結果は泳動速度の実験結果と良く一致した．このときの Re 数は 10^{-6} と，低 Re 条件下においてよく一致した結果が得られた．Fig. 6 に周波数に対する負荷トルクの解析結果を示す．実験の条件から，磁気トルクが 66 μNm であるので，

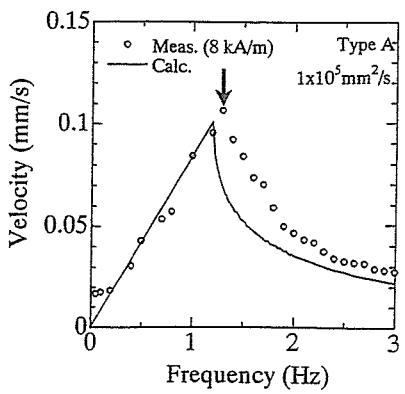

Fig. 5 Relation between frequency and swimming velocity of Type A.

このとき負荷トルクの解析結果から得られる駆動可能周波数範囲は 1.2 Hz となり，実験結果と良く一致した結果が得られた．

B. Type B

Fig. 7 に周波数に対する泳動速度の解析結果を示す．図中のプロットは，実験結果であり，実線は 3 次元解析である．図中の矢印は，実験における脱調周波数を示し 2.4 Hz

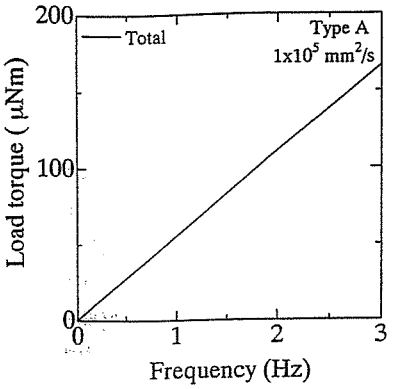

Fig. 6 Relation between frequency and load torque of Type A.

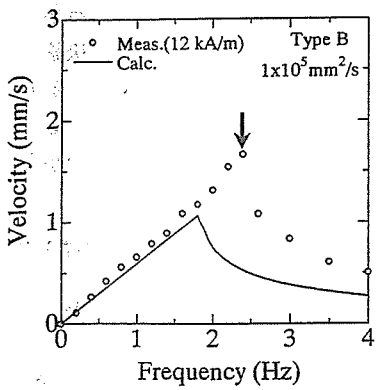

Fig. 7 Relation between frequency and swimming velocity of Type B.

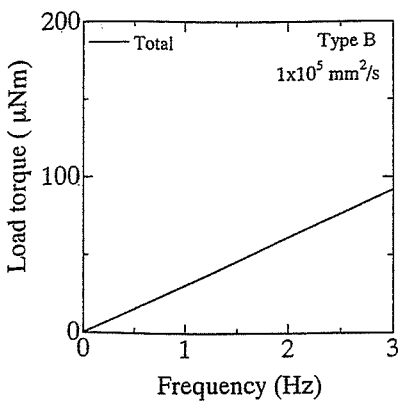

Fig. 8 Relation between frequency and load torque of Type B.

であった．脱調周波数以前においては，実験結果と 3 次元解析は一致した結果が得られた．Fig. 8 に周波数に対する負荷トルクの解析結果を示す．実験の条件から，磁気トルクが 58 μNm であるので，このとき負荷トルクの解析結果から得られる駆動可能周波数範囲は 1.8 Hz となり，実験と解析の結果に 25 %の誤差が生じた．そのため Fig. 7 に示す泳動速度の結果において，脱調後の軌跡にずれが生じている．

3. まとめ

スパイラル型磁気マイクロマシンの泳動特性を有限体積法を用いて 3 次元解析を行った．この解析方法を用いて，マシン周辺の速度分布，圧力分布を求めることができた．これらの速度分布，圧力分布を用いて，推力，抗力，負荷トルク，泳動速度を求めた．マシンの脱調後の泳動速度については，マシン回転方向の方程式をルンゲ・クッタ法で解き，脱調後のマシンの平均回転周波数を求め，泳動速度を求めた．解析結果の妥当性を検討するためマシンの推進と回転方向成分の解析結果をそれぞれ泳動速度，脱調周波数の実験結果と比較した．その結果，Type A に関しては，脱調前後において泳動速度と脱調周波数の解析結果が実験と一致した．Type B に関しては，脱調前における泳動速度の実験と解析結果は一致したことから，推進方向の解析結果の妥当性は示された．しかしながら，解析と実験結果の脱調周波数には 25 %の誤差が生じた．解析による脱調周波数は，回転方向成分である負荷トルクの結果を用いて求めるため，回転方向に関しては誤差が生じた．

3 次元解析は 2 次元解析に比べ計算量，計算時間が多い．一方で 3 次元解析はフィッティングパラメータを使用せず，低 Re 領域まで解析が可能であることが示された．従って，3 次元解析手法を用いることで，解析のみのマシン設計を行うことが可能となる．

文献

1) M. Sendoh, N. Ajiro, K. Ishiyama, M. Inoue, K. I. Arai, IEEE Trans. Magn. 36, 3688 (1999).
2) M. Sendoh, A. Yamazaki, K. Ishiyama, M. Inoue, T. Hayase, K. I. Arai, J. Mag. Soc. Jan., 25, 1223 (2001).
3) T. Hayase, J. A. C. Humphrey, R. Greif, J. Heat Trans., 114, 589 (1992).
4) Douglas John Goering, Ph.D. Dissertation at the University of California, Berkeley, 1989.
5) S. V. Patankar, Numerical heat Transfer and Fluid Flow, Hemisphere, 1980.
6) T. Hayase, J. A. C. Humphrey, R. Greif, J. Comput. Phys., 98-1, 108 (1992).
7) M. Sendoh, K. Ishiyama, M. Yamaguchi, K. I. Arai, J. Mag. Soc. Jan., 26, 653 (2002).

2002 年 10 月 7 日受理，2002 年 11 月 20 日採録

日本応用磁気学会誌 27, 681–685 (2003)

〈論 文〉

低温フェライトめっき技術の磁気マイクロマシンへの応用

Application of a Magnetic Micro-machine to a Low-temperature Ferrite Plating Technique

西村一寛・仙道雅彦*・石山和志*・荒井賢一*・内田裕久・井上光輝

豊橋技術科学大学工学部電気・電子工学系，豊橋市天伯町雲雀ヶ丘 1-1 (〒441-8580)
*東北大学電気通信研究所，仙台市青葉区片平 2-1-1 (〒980-8577)

K. Nishimura, M. Sendoh*, K. Ishiyama*, K. I. Arai*, and M. Inoue

Department of Electrical & Electronic Engineering, Toyohashi University of Technology, *1-1 Tenpaku-cho, Toyohashi 441-8580*
*Research Institute of Electrical Communication, Tohoku University, *2-1-1 Katahira, Aoba-ku, Sendai 980-8577*

By using a ferrite plating technique and stereolithography, we fabricated the medical magnetic micro-machines that plated ferrites on a spiral-structured resinous substrate. We plated a magnetite (Fe_3O_4) film with good biocompatibility and $Co_xFe_{3-x}O_4$ films ($Co_{0.39}Fe_{2.61}O_4$ or $Co_{0.45}Fe_{2.55}O_4$) having large coercive force onto template bodies at 90 °C for 5–8 hours, and fabricated solid-state-based ferrite-coated micro-machines with biocompatibility and light mass density. All the micro-machines were able to swim in water when an external rotational magnetic field was applied.

Key words: ferrite plating, Fe_3O_4, stereolithography, micro-machine, biocompatibility

1. はじめに

磁気力によって駆動するマイクロマシンは，駆動のための電源が外部磁場によって供給できるため，体内中での遠隔治療などの応用が期待されている．このマイクロマシンの開発[1]は，螺旋構造をした泳動型のものが，セラミックパイプ，タングステンワイヤーのスパイラルブレイド，希土類磁石を用いて試作されたり，光造形法より作製された螺旋構造をした樹脂と希土類磁石を用いて試作されたりしている．いずれのマシンにおいても，良好な駆動特性を得ることに成功しているが，比重が大きく希土類磁石はすぐに錆びてしまうなど体内注入型のマイクロマシンとしての機能が完全とは言えない．

マイクロマシンを，体液や血液中を自由に移動させるためには，小型化が可能なこと，生体適合性が高いことが必要とされる．さらに，その比重を体液や血液と等しくすることで重力の影響がなく制御しやすいものとなる．

そこで，微細加工が可能な光造形法を用いた螺旋構造をした樹脂を用いることによって，小型化の可能性および比重を小さくし，さらにフェライトをコーティングすることで，化学的安定性および生体適合性を持つ薄膜型の医療磁性マイクロマシンの作製を提案する．樹脂材料を利用することでマシンが柔らかくなり血管等へ傷をつけたりすることが緩和されることも期待できる．

本研究では，フェライトには生体適合性[2]が報告されているマグネタイト(Fe_3O_4)，および磁石材料として Co イオンが固溶した $Co_xFe_{3-x}O_4$ を取り上げめっきした．フェライトめっきについての詳細は著者らの報告[3]を参照されたい．特に，磁石材料の $Co_xFe_{3-x}O_4$ については，結晶化していれば Co^{2+}イオンの固溶量を増加させることによって保磁力が増加することが予想されるため，Co 固溶量が最も大きくなるものを調査した．これらの結果を基にして，フェライトをコートしたマイクロマシンを試作し，それらの磁気特性，泳動特性を調査した．

2. 実験方法

Fig. 1 に示すプラスティック製容器(容積 100 cm^3)を用い，19.5 kHz, 600 W の強力超音波を印加することによって実験を行った．容器内には，マイクロマシン用樹脂および，参照用のスライドガラス(3.7 cm×2.5 cm×0.11 cm)を水に浸るように入れ，金属イオンを溶した反応液と，酸化剤および pH 調整剤を溶した酸化液をどちらも同じ流量 3ml/min で導入し，常に新鮮な溶液に保つため排出した．**Table 1** に示すような薬品を反応液と酸化液に用いた．反応液には，Fe_3O_4 膜を作製する場合は，$FeCl_2$ のみを用い，Co を固溶させた $Co_xFe_{3-x}O_4$ 膜を作製する場合は，さらに $CoCl_2$ を添加することで行う．特に，この場合 $FeCl_3$ を添加させることも行った．

金属イオンの濃度は，トータルで 0.1 mol/l になるようにした．酸化液の pH 調整剤には，反応時の pH 値がおよそ 6 となるように，$CH_3COONH_4 + NH_4OH$ を用い，酸化剤には，$NaNO_2$ を

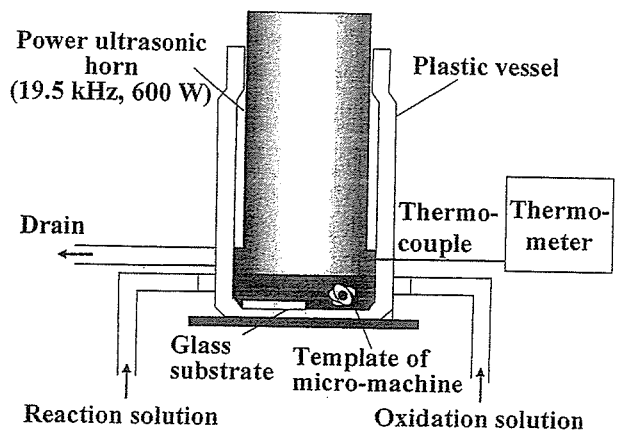

Fig. 1 Apparatus for ultrasound-enhanced ferrite plating.

Table 1 Chemicals used in ferrite plating.

	Chemicals (mol/l)	
Reaction solution	$FeCl_2$	$0.1-x-y$
	$xCoCl_2$	0 – 0.033
	$yFeCl_3$	0 – 0.003
	Total	0.1 mol/l
Oxidation solution	CH_3COONH_4	1.0
	NH_4OH	0 – 0.002
	$NaNO_2$	0.01

用いた. ここで CH_3COONH_4 は pH 緩衝剤であり金属イオンの濃度の 10 倍とした. 温度は, 超音波の印加する強度を調整することでおよそ 90 °C に保たれる.

作製した膜は, X 線回折装置によって結晶構造を同定し, 試料振動型磁力計によって磁気特性を測定した. 膜の組成は, EDX を用いて同定した. 膜厚は, FE-SEM によって断面を観察することによって測定した.

3. 実験結果

マイクロマシン用樹脂へのめっきの前にガラス基板を用いて, Fe_3O_4, Co を固溶した $Co_xFe_{3-x}O_4$ 膜の堆積を行った. Fig. 2 には, ○は M^{2+}イオン(M = Fe, Co)のみを用いたもの, ●は Fe^{3+}イオンを全金属イオンの 3%とわずかに添加したものについて, 横軸に溶液中の $Co_xFe_{3-x}O_4$ 組成, 縦軸に膜中の組成を取ったものを示す. 膜中への Co^{2+}の取り込み量は, 仕込み溶液の半分程度で Fe^{3+}イオンを添加したものの方がわずかに多い. このことについての詳細は, 過去に報告したフェライトめっきにおける組成[3]や Fe^{3+}イオンの添加効果[4]を参照されたい.

Fig. 3(A)より, 最大±10kOe 印加した場合の磁化は, M^{2+}

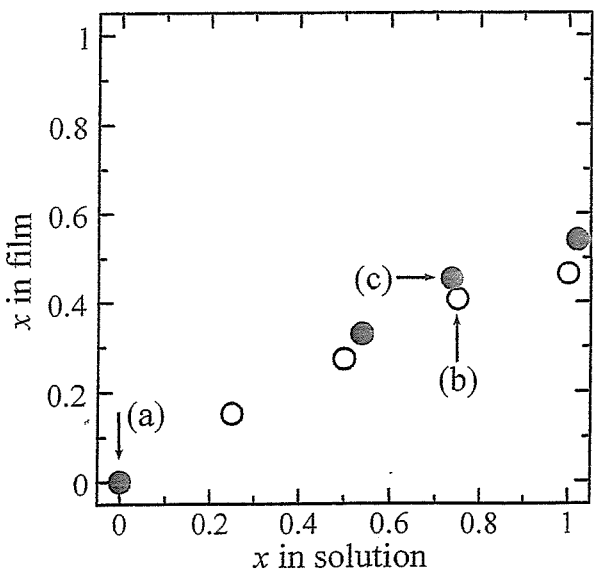

Fig. 2 Concentration x in $Co_xFe_{3-x}O_4$ films of the spinel structure plated using Fe^{3+} ions (closed circles) and without them (open circles), plotted as a function of x in reaction solution.

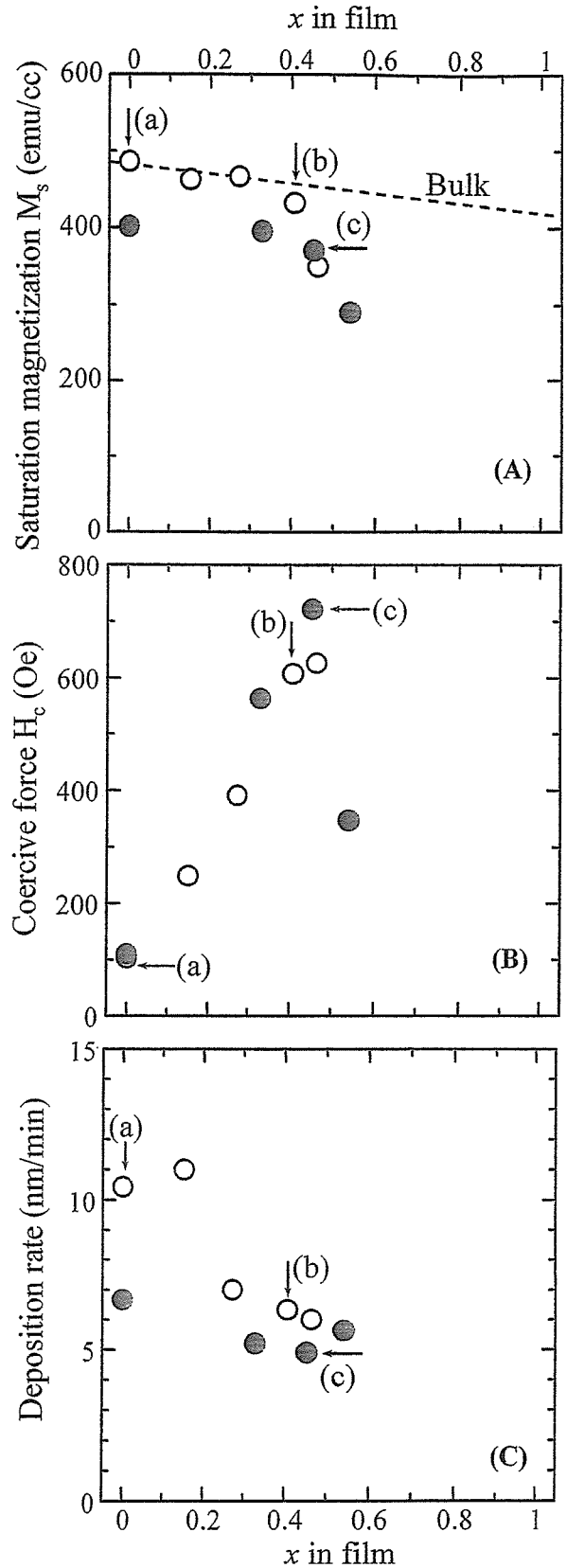

Fig. 3 Saturation magnetization (A), coercive force (B), and deposition rate (C) of the spinel structure plated using Fe^{3+} ions (closed circles) and without using them (open circles), plotted as a function of x in $Co_xFe_{3-x}O_4$ films.

イオンを用いた場合（図中の○）は，バルク文献値(M_s = 480 emu/cc for Fe_3O_4, M_s = 420 emu/cc for $CoFe_2O_4$)にほぼ等しい値となった．Fe^{3+}イオンを添加した●は，バルク文献値の８割程度となった．これは，Fe^{3+}イオンを添加することによって結晶化は促進されるが微粒子も多量に発生し[4]，そのため膜は荒れ少し密度が悪くなったことが考えられる．保磁力は，Fig. 3(B)より，スピネル構造を持ったものでは，膜中の組成xの増加にしたがって大きくなっている．Fe^{3+}イオンを添加したもの(H_c = 720 Oe)では，M^{2+}イオンのみのもの(H_c = 630 Oe)よりも大きな保磁力になった．堆積速度は，Fig. 3(C)のようにFe^{3+}イオンを添加したものは遅くなるが，いずれの場合もCoイオンの固溶量の増大によっても遅くなった．

Fig. 4 には，(A)はM^{2+}イオンのみを用いたもの，(B)はFe^{3+}イオンを添加したものについて，作製した膜のX線回折結果を示した．Fe^{3+}を添加することで微粒子が形成しやすく微細化するため[4]結晶構造はブロードになっている

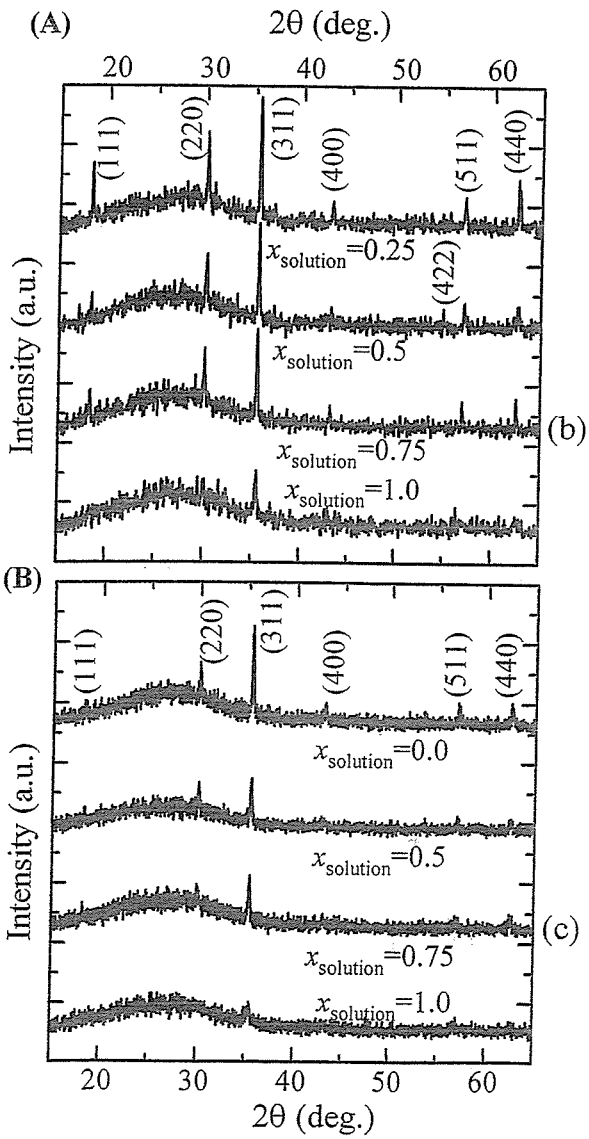

Fig. 4 XRD diagrams for films plated (A) using only M^{2+} ions and (B) using Fe^{3+} ions.

が，(A), (B) ともに典型的なスピネル構造であった．いずれの場合においても，溶液中の Co の組成xを増加するに従い結晶構造が悪くなり，x=1.0 においては，アモルファス化している．この場合の磁化は，Fig. 3(A)に示すように小さい．これら薄膜の磁気特性および結晶構造により，Fe^{2+}イオンのみを用いて作製したFe_3O_4, M^{2+}イオンを用いて作製した Co を固溶したもの，Fe^{3+}を添加して作製した Co を固溶したものを，それぞれ，図中の(a), (b), (c)の３つの作製条件よりマイクロマシンを作製した．

Fig. 5 には，螺旋構造をした樹脂にめっきしたものの磁化曲線を示す．Fig. 5 の矢印方向に測定をした．Fig. 5(a)は，Fe^{2+}イオンのみで 533 分間めっきしたもので，保磁力は 60 Oe とソフトな磁気特性を示した．Fig. 5(b)は，M^{2+}イオンのみで300分間作製したCoを固溶したもので，EDXの結果，$Co_{0.39}Fe_{2.61}O_4$ であることを同定した．保磁力は，860 Oe であった．Fig. 5(c)は，Fe^{3+}を添加して 333 分間作製した Co を固溶したもので，EDX で，$Co_{0.45}Fe_{2.55}O_4$ であることを同定した．保磁力は，1060 Oe であった．これらマシンの磁化量は，めっき時間を長くすることによって剥離しなければ増加させることが可能である．

これら３種類のマシンを Fig. 6 の矢印方向に着磁を行い純水中での泳動特性を周波数，回転磁界の強度をパラメータに取ったものを Fig. 6 に示す．泳動特性は，４回以上測定しその平均値を取った．Fig. 6(a)は，軟磁気特性を示したFe_3O_4をコーティングしたマシンの泳動特性を示したもので，保磁力以下の回転磁場を印加しても駆動しないが，保磁力以上の周波数では駆動している．保磁力以下では，自発磁化によって外部回転磁場に同期して回転することが考えられたが，実際は磁化が減少してしまい駆動する動力が得られなかったことが駆動できない原因だと考えられる．十分に磁化が得られる回転磁場の強度では回転磁場に同期して動作すると考えられる．低い周波数 20 Hz 未満で動作しないが，非常に興味深い泳動特性が得られた．Fig. 6(b), (c)の泳動特性は，励磁周波数とともに泳動速度が増加し，ある周波数でマシン回転が回転磁界に追従できなくなり脱調している．脱調周波数は，印加磁界強度とともに増加している．これは，着磁によって磁化されたマシンが外部回転磁界と同期することによってトルクが得られマシンが回転するためであり，脱調は，速度に追従するトルクが得られないため起こると考えられる．そのため，外部回転磁場の強度を大きくすることで脱調周波数は増加する．また，脱調周波数以下においてマシンの泳動速度は磁界強度に依存しなかった．これは，マシンが回転磁界に同期して回転しているためである．この泳動特性は，磁石材料を用いた従来の研究のもの[1]と同じ傾向である．しかしながら，従来のマシンは比重が大きいため粘性溶液中での駆動であるのに対して，水中で駆動できることが大きな特長であり，樹脂材料にコートしたマシンの比重が小さいことを示している．

また，これら(a), (b), (c)はそれぞれ異なる泳動特性を示

すことから，同一溶液中で複数個のマシンを個別に駆動させることも期待できる．

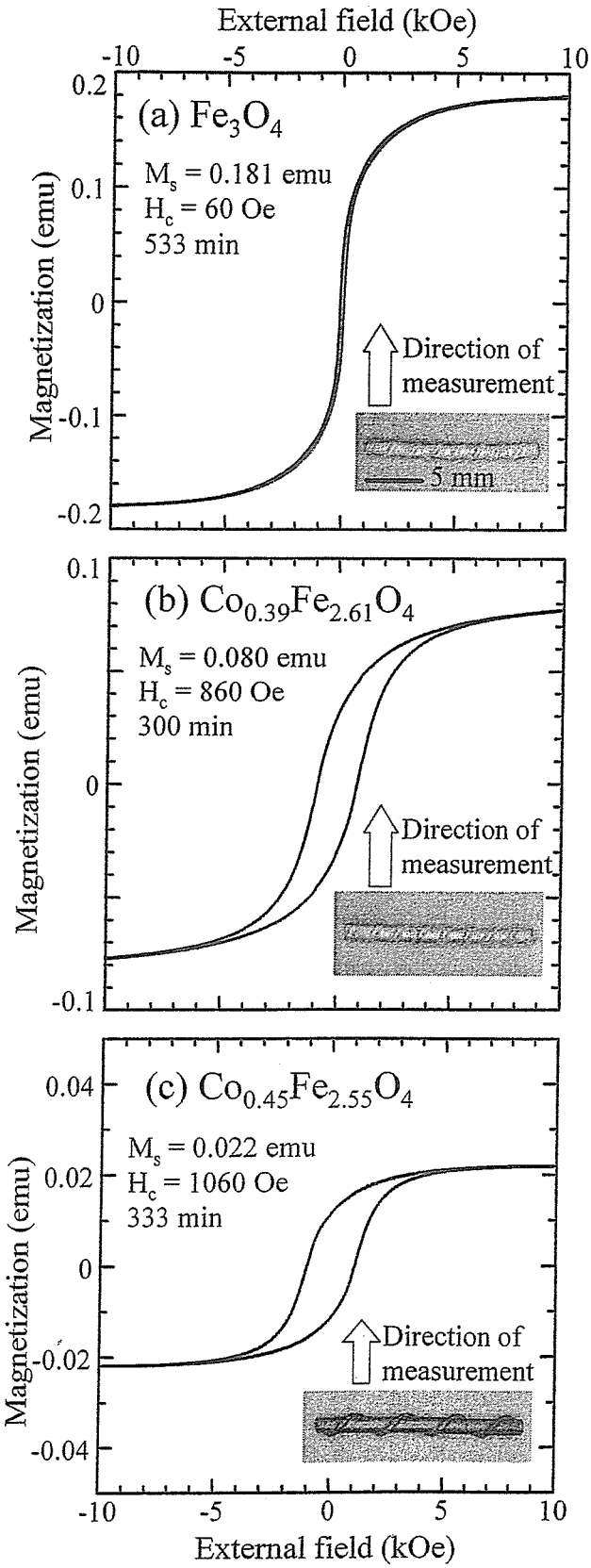

Fig. 5 Magnetization curves for machines plated with (a) Fe_3O_4, (b) $Co_{0.39}Fe_{2.61}O_4$, and (c) $Co_{0.45}Fe_{2.55}O_4$.

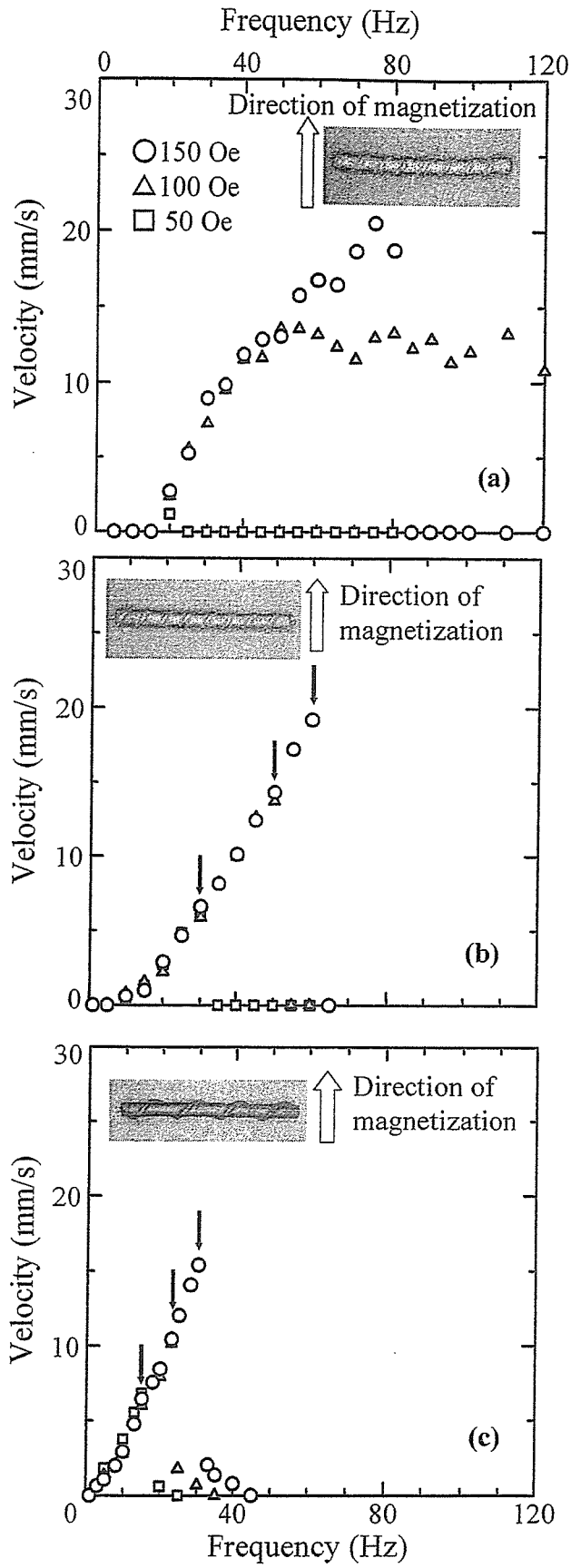

Fig.6 Swimming velocity of a machine plated with (a) Fe_3O_4, (b) $Co_{0.39}Fe_{2.61}O_4$, and (c) $Co_{0.45}Fe_{2.55}O_4$, plotted as a function of the frequency.

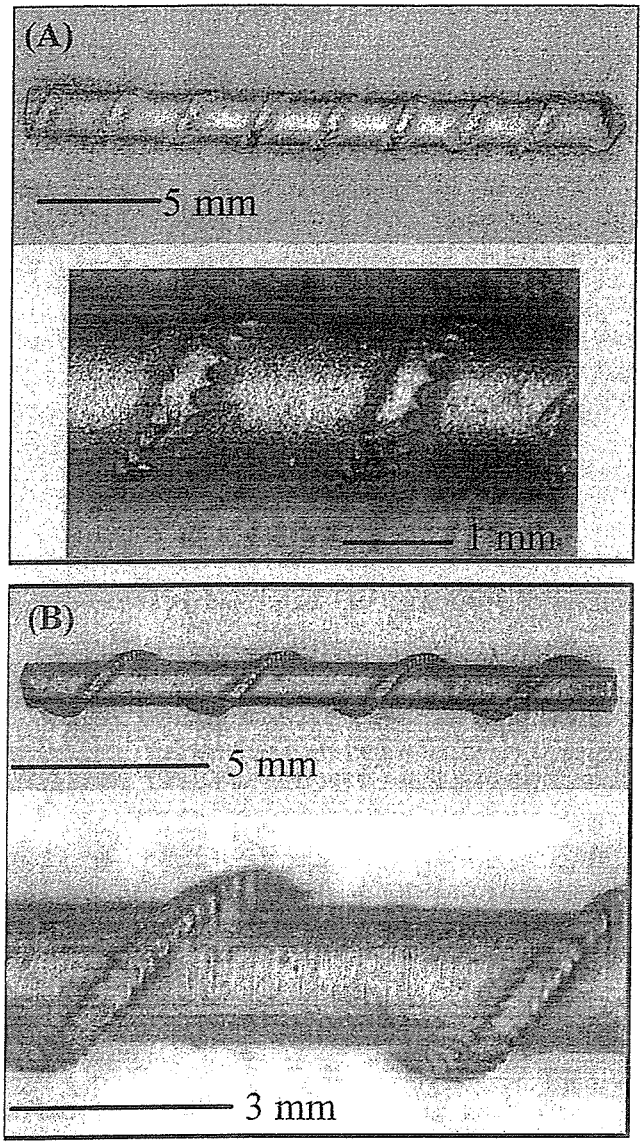

Fig. 7 Photos of (A) $Co_{0.39}Fe_{2.61}O_4$ and (B) $Co_{0.45}Fe_{2.55}O_4$.

作製したマシンは，Fig. 7 の(A), (B)に示すように，非常に微細なブレードに陰影効果なく均一にめっきされていることが確認できた．

4. まとめ

本報告によって，

（1） Fe^{3+}イオンを添加することによって，堆積速度が少し減少するが，保磁力が，M^{2+}イオンのみを用いて作製した場合に比べて大きなものを作製することに成功した．

（2） Fe_3O_4, $Co_{0.39}Fe_{2.61}O_4$, $Co_{0.45}Fe_{2.55}O_4$ の３つの異なる磁気特性をもつマイクロマシンを作製し，生体適合性をもつFe_3O_4をコートしたマシンでは外部回転磁界 100Oe 以上，回転周波数 20Hz 以上で駆動を確認した．Co を固溶した高保磁力のフェライトをコートしたマシンは，従来の磁石を用いるものと同じような泳動特性となった．

（3） 作製した全てのマシンは，沈むことなく水中を泳動することを確認した．

（4） 複雑な構造をした樹脂に陰影効果なく均一にコーティングできることを確認した．

以上，光造形法によって作製した螺旋構造をした樹脂にフェライトをコーティングすることによって，水中を泳動できる薄膜型の磁気マイクロマシンを開発した．実際の血管で動作させるにはサブ mm 程度に小型化する必要がある．さらなる小型化を目指して，最新の光造形技術を用いた加工（数μm 程度）[5]，螺旋構造に類似した昆虫の触覚，バクテリアのべん毛（全長数μm 程度）[6,7]，カーボンナノコイル，螺旋構造をもつＤＮＡなどを用いてフェライトめっきすることを検討している．

謝 辞 本研究は文部科学省２１世紀 COE プログラム「インテリジェント ヒューマンセンシング」の援助により行われた．また，光造形によるマシンの試作において多大な御協力を頂いた，通商産業省工業技術院 機械技術研究所，明渡純氏ならびに谷川民生氏に深く感謝致します．

文 献

1) 例えば， 仙道雅彦・石山和志・山口正洋・荒井賢一：日本応用磁気学会誌，**26**, 653 (2002)
2) F. Miyawaki, T. Tsuji, M. Abe, and M. Kaibara: Proc. XIII World Congress of Cardiology, ed. by Monduzzi, Rio de Janeiro (Brazil), 1998, p. 1133.
3) 西村一寛，松下伸広，阿部正紀：日本応用磁気学会誌，**25**, 879 (2001).
4) 西村一寛，畑中真二，松下伸広，阿部正紀：日本応用磁気学会誌，**26**, 457 (2002).
5) S. Maruo and K. Ikuta, Appl. Phys. Lett., **76**, 2625 (2000).
6) D. J. DeRosier, Cell, **93**, 17 (1998).
7) L. Turner, S. W. S. Ryu, and H. C. Berg, J. Bacteriol., **182**, 2793 (2000).

2002 年 12 月 27 日受理，2003 年 3 月 26 日採録

Available online at www.sciencedirect.com
SCIENCE DIRECT®
Sensors and Actuators A 105 (2003) 103–108
SENSORS AND ACTUATORS A PHYSICAL
www.elsevier.com/locate/sna

Three-dimensional analysis of swimming properties of a spiral-type magnetic micro-machine

A. Yamazaki [a,*], M. Sendoh [a], K. Ishiyama [a], T. Hayase [b], K.I. Arai [a]

[a] *Research Institute of Electrical Communication, Tohoku University, 2-1-1 Katahira Aoba-ku, Sendai 980-8577, Japan*
[b] *Institute of Fluid Science, Tohoku University, 2-1-1 Katahira Aoba-ku, Sendai 980-8577, Japan*

Received 23 July 2002; received in revised form 26 October 2002; accepted 26 February 2003

Abstract

The swimming properties of a spiral-type magnetic micro-machine were analyzed theoretically using 3D finite volume method. The basic equations of incompressible viscous fluid flow were integrated. The flow field around the micro-machine was calculated to estimate the swimming velocity, thrust, drag, and load torque of a spiral-type magnetic micro-machine. Good agreement was obtained between the experimental and theoretical results in a low Reynolds number. Therefore, the 3D analysis method without any fitting parameters was judged to be established.

Keywords: Micro-machine; Spiral blade; Rotating magnetic field; Finite volume method

1. Introduction

Magnetic micro-machines require no power supply cables, no batteries, and no controlling systems on the machine body. These advantages are expected to lead to the application of medical micro-machines in new medical-treatment technologies, such as minimally invasive surgeries and drug delivery systems. In this case, the micro-machine moves in the human body. As some organs are filled with liquids such as blood, the swimming mechanisms of micro-machines must be examined.

In previous studies, we examined the swimming properties of a spiral-type magnetic micro-machine [1,2]. Fig. 1 shows a schematic view of the micro-machine. The machine was composed of a cylindrical magnet and a spiral blade. As the magnet was magnetized in the radial direction, the machine rotated in synch with the rotating external magnetic field. We established a method for the two-dimensional (2D) analysis of swimming properties of the micro-machine by means of the finite volume method [1]. The experimental and analytical results were in close agreement under a very wide-range of the Reynolds number conditions ($10^{-7} < Re < 10^{3}$) [1,2]. Consequently, we found that the spiral-type structure and method for 2D analysis was applicable under a very wide-range of Reynolds numbers. However, this method for 2D analysis required a fitting parameter to fit the experimental results. In our previous study, a thickness of the boundary layer was used as this fitting parameter. Therefore, 3D analysis method without any fitting parameter is required. In general studies, 3D analysis method applicable to a high Reynolds number is established. However, 3D analysis method applicable to the swimming micro-machine in a low Reynolds number is not established.

In this study, we theoretically analyzed the swimming properties of a spiral-type magnetic micro-machine using the 3D finite volume method without any fitting parameters. We examined this analysis method and compared its result with results obtained from experiments.

2. Three-dimensional analysis of the micro-machine

2.1. Micro-machine

Fig. 1 shows the size of the micro-machine used in this analysis. The micro-machine had a body diameter of 1.2 mm, length of 15 mm, blade height of 0.15 mm, and pitch of 4.4 mm. Fig. 2 shows a photograph of the spiral-type magnetic micro-machine used for the experiment [2]. The micro-machine was composed of two ceramic pipes, connected at both the ends of a cylindrical NdFeB magnet measuring 1.2 mm in diameter and length of 7.5 mm. The

* Corresponding author. Tel.: +81-2-221-754-88; fax: +81-2-221-75-728.
E-mail address: aya@riec.tohoku.ac.jp (A. Yamazaki).

0924-4247/03/$ – see front matter © 2003 Elsevier Science B.V. All rights reserved.
doi:10.1016/S0924-4247(03)00069-4

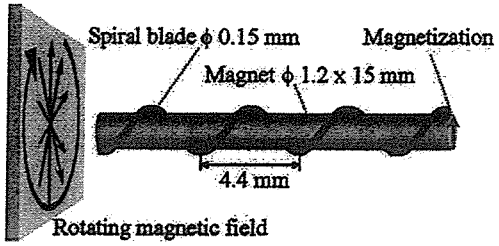

Fig. 1. Schematic view of spiral-type of micro-machine.

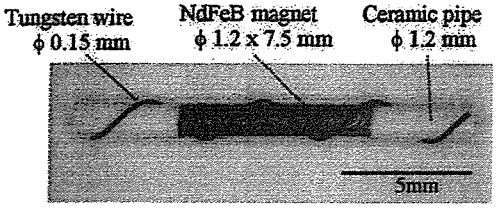

Fig. 2. The photograph of the spiral-type magnetic micro-machine used for the experiment.

micro-machine itself spanned a length of 15 mm. A tungsten wire with a diameter of 0.15 mm was wound around the body, and the pitch of the spiral blade was 4.4 mm. The magnet used for the experiment had a residual magnetization of 0.98 T, and the strength of the applied magnetic field in the experiment was 8 kA/m (100 Oe). The magnetic torque was calculated by the product of the magnetic moment on the micro-machine and the intensity of the magnetic field in the experiment. Using this calculation, the maximum magnetic torque was 66 μN m.

2.2. Three-dimensional and two-dimensional analyses

Fig. 3 shows a simplified model used in 2D analysis, and Fig. 4 shows a simplified model used in 3D analysis. In both of the analysis models we set the z-axis as the central axis of the micro-machine and the external wall in the place of

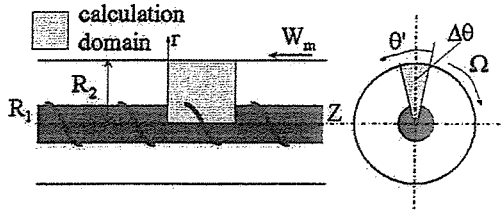

Fig. 3. Simplified model used in the 2D analysis.

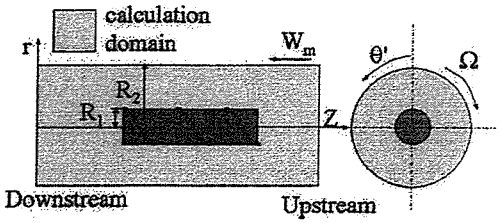

Fig. 4. Simplified model used in the 3D analysis.

a radius R_2. To simulate the swimming and rotation of the micro-machine, we used a set of cylindrical coordinates (r, θ, z) that moved and rotated with the micro-machine. The treatment of the micro-machine length constituted the principal difference between the 2D and 3D analyses. In the 2D analysis, the length of the micro-machine was treated as an infinite length, and one spiral was calculated assuming periodicity. Since the micro-machine had no ends, the boundary layer could not be exactly expressed. The external wall ($r = R_2$) was located as the thickness of the boundary layer and treated as a fitting parameter. The value was set based on a reference value obtained from the experiment. The effect of both ends of the micro-machine on the drag was treated as that of a disk with the same diameter as the micro-machine. In 3D analysis, the length of the micro-machine was treated as finite length, and the calculation domain was set around the micro-machine. The boundary layer could be expressed exactly and the effect of both ends of the micro-machine was calculated well. Thus, there was no need to use a fitting parameter within the analysis.

2.3. Basic equation

Velocity components (u, v', w') and coordinates (r, θ', z') are related to those on stationary coordinates as,

$$\left.\begin{aligned}\theta &= \theta' + \Omega t\\ z &= z' + W_m t\end{aligned}\right\} \tag{1}$$

$$\left.\begin{aligned}v &= v' + \Omega r\\ w &= w' + W_m\end{aligned}\right\} \tag{2}$$

where Ω and W_m are the angular velocity of rotation and swimming velocity of the micro-machine. In an incompressible viscous fluid, a steady Navier–Stokes equation is written as follows from Eqs. (1) and (2) [3].

$$u\frac{\partial u}{\partial r} + \frac{v'}{r}\frac{\partial u}{\partial \theta'} + w'\frac{\partial u}{\partial z'} + W_m\frac{\partial u}{\partial z'} - \frac{v'^2}{r} - 2\Omega v' - r\Omega^2 = -\frac{\partial p}{\partial r} + \frac{1}{Re} \times \left(\frac{\partial^2 u}{\partial r^2} + \frac{1}{r}\frac{\partial u}{\partial r} - \frac{u}{r^2} + \frac{1}{r^2}\frac{\partial^2 u}{\partial \theta'^2} - \frac{2}{r^2}\frac{\partial v'}{\partial \theta'} + \frac{\partial^2 u}{\partial z'^2}\right) \tag{3}$$

$$u\frac{\partial v'}{\partial r} + \frac{v'}{r}\frac{\partial v'}{\partial \theta'} + w'\frac{\partial v'}{\partial z'} + W_m\frac{\partial v'}{\partial z'} + \frac{uv'}{r} + 2\Omega u = -\frac{1}{r}\frac{\partial p}{\partial \theta'} + \frac{1}{Re} \times \left(\frac{\partial^2 v'}{\partial r^2} + \frac{1}{r}\frac{\partial v'}{\partial r} - \frac{v'}{r^2} + \frac{1}{r^2}\frac{\partial^2 v'}{\partial \theta'^2} + \frac{2}{r^2}\frac{\partial u}{\partial \theta'} + \frac{\partial^2 v'}{\partial z'^2}\right) \tag{4}$$

$$u\frac{\partial w'}{\partial r} + \frac{v'}{r}\frac{\partial w'}{\partial \theta'} + w'\frac{\partial w'}{\partial z'} + W_m\frac{\partial w'}{\partial z'} = -\frac{\partial p}{\partial z'} + \frac{1}{Re}\left(\frac{\partial^2 w'}{\partial r^2} + \frac{1}{r}\frac{\partial w'}{\partial r} + \frac{1}{r^2}\frac{\partial w'}{\partial \theta'^2} + \frac{\partial^2 w'}{\partial z'^2}\right) \tag{5}$$

Re in Eqs. (3)–(5) is the Reynolds number

$$Re = \frac{\tilde{\Omega}\tilde{R}_1^2}{\tilde{\nu}} \tag{6}$$

where $\tilde{\nu}$ is the kinematic viscosity of the liquid, and $\tilde{R}_1$ the radius of the body. The equation of continuity is written as

$$\frac{\partial u}{\partial r} + \frac{u}{r} + \frac{1}{r}\frac{\partial v'}{\partial \theta'} + \frac{\partial w'}{\partial z'} = 0 \tag{7}$$

The basic equations are written with dimensionless quantities. Here, the representative velocity, length, and pressure are $\tilde{\Omega}\tilde{R}_1$, $\tilde{R}_1$ and $\tilde{\rho}(\tilde{\Omega}\tilde{R}_1)^2$, respectively, and the fluid density is $\tilde{\rho}$.

Boundary conditions on solid walls are given by the no-slip condition written as

Outer wall

$$\begin{cases} u(R_2, \theta, z) = 0 \\ v'(R_2, \theta, z) = -\Omega R_2 \\ w'(R_2, \theta, z) = -W_m \end{cases} \tag{8}$$

Machine surface

$$\begin{cases} u = 0 \\ v' = 0 \\ w' = 0 \end{cases} \tag{9}$$

On the upstream boundary, null velocity is assumed on the stationary coordinate system. This condition is transformed to the uniform axial flow with a solid body rotation as,

$$\begin{cases} u = 0 \\ v' = -\Omega r \\ w' = -W_m \end{cases} \tag{10}$$

On the downstream boundary, free stream condition is applied as,

$$\begin{cases} \dfrac{\partial u}{\partial z'} = 0 \\ \dfrac{\partial v'}{\partial z'} = 0 \\ \dfrac{\partial w'}{\partial z'} = 0 \end{cases} \tag{11}$$

Singularity on the z-axis is treated as the reference [4].

2.4. Calculation

The basic equations were discretized by finite volume method using a staggered grid system. A method similar to the SIMPLER method [5] was used to solve discretized equations. The reformulated QUICK scheme [6] was used to discretize the convective terms of the Navier–Stokes equation. Parallel computing was performed in an analysis using four CPUs of a SGI Origin 2000 supercomputer installed at the Institute of Fluid Science in Tohoku University. About 590,000 grid points were included in the analysis. It took the CPUs about 160 h to perform the calculation.

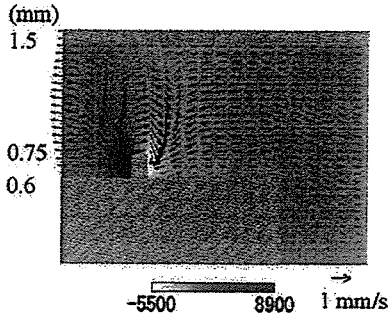

Fig. 5. Visualization of the solved flow field.

Fig. 5 is a visualization of the solved flow fields. The arrows in the figure show the velocity of the fluid, and the background color shows the distribution of pressure. The slash is the micro-machine and external wall. When the micro-machine travels in a frontward direction in this figure, there was a high pressure difference between the front and back of the spiral blade at the rear side. The thrust and the load torque are calculated from the axial and tangential component of the force acting on the spiral blade, respectively. Using the calculated velocity distribution, the load torque and drag are calculated from the viscous shear stress on the micro-machine surface. When taking the distribution $u(y)$ as the flow on a certain wall surface, as shown in Fig. 6 (from the conditions of no-slip, the flow velocity is 0 on the object surface), the viscous shear stress τ on the wall is written as [7]

$$\tau = \mu \left.\frac{\partial u}{\partial y}\right|_{y=0} \tag{12}$$

Here, μ is the coefficient of viscosity. Using u_1, u_2, h in this figure, the second-order-accurate formula of the wall shear stress τ is written as [6]

$$\tau = \mu \frac{9u_1 - u_2}{6h} \tag{13}$$

Next, we calculated the extent to which the viscous shear stress obtained from Eq. (13) acted on the micro-machine surface. To perform this calculation, we needed to know the drag and load torque generated by the viscous shear stress. The pressure difference between the front and back of the ends of the micro-machine was set as the thrust, and the torque generated by the viscous stress of the ends of the

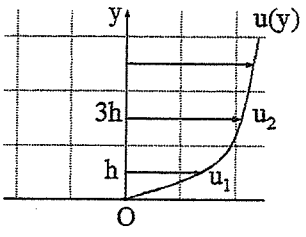

Fig. 6. The velocity distribution $u(y)$ of the flow on a solid wall surface.

micro-machine was set as the load torque. When the thrust of the micro-machine was equal to drag, the swimming velocity of the micro-machine was set as the velocity of the external wall (W_m).

The load torque increased together with the frequency. When the load torque exceeded the magnetic torque, the rotation of the micro-machine did not synchronize with the rotating external field. The frequency at this time is called step-out frequency. Over the step-out frequency, the micro-machine proceeded forward with intermittent step-out. Therefore, the average rotation frequency of the micro-machine over the step-out frequency falls below the frequency of the rotating external magnet field. The equations for the micro-machine rotation direction were solved using the Runge–Kutta method [8]. The average rotation frequency of the micro-machine cannot be defined without solving these equations. The equations of the micro-machine rotation direction are written as

$$MH\sin(\omega t - \theta) = J\frac{d^2\theta}{dt^2} + D_f\frac{d\theta}{dt} \quad (14)$$

M is the magnetization, H the external magnetic field, ω the angular frequency of external magnetic field, θ the rotation angle of the machine, J the moment of inertia, and D_f the proportionality factor showing the relation between load torque and rotation velocity.

The left side of Eq. (14) is magnetic torque, the first term on the right side is inertia power, and the second term on the right side is the load torque received from the fluid. The proportionality factor D_f was decided from the graph on the relation between the frequency and the load torque that the 3D analysis sought to solve. The swimming velocity over the step-out frequency was taken as the swimming velocity at the average rotation frequency of the machine.

2.5. Analysis result and discussion

We used two types of liquids with kinematic viscosity listed in Table 1. Fig. 7 shows the relation between the frequency and the swimming velocity of the micro-machine. In this figure, the open circle plots the experimental result obtained in our previous work [2], and the solid line plots the analysis result. The calculated result agrees with the experimental one. The swimming velocity increases in proportion to the frequency. The arrowhead in this figure shows step-out frequency. The step-out frequencies in the liquids with kinematic viscosities of 1×10^5 and 5×10^5 mm^2/s are 1.3 and 0.24 Hz, respectively. The Reynolds number in this point is 1×10^{-6} and 1×10^{-7}, respectively. These results indicated the analytical results agreed with the experimental results in a low Reynolds number.

Table 1
Liquids used in the study

Kind of liquid	Kinematic viscocity ν (mm^2/s)	Density ρ (10^3 kg/m^3)
Silicon oil	1×10^5	0.967
Silicon oil	5×10^5	0.967

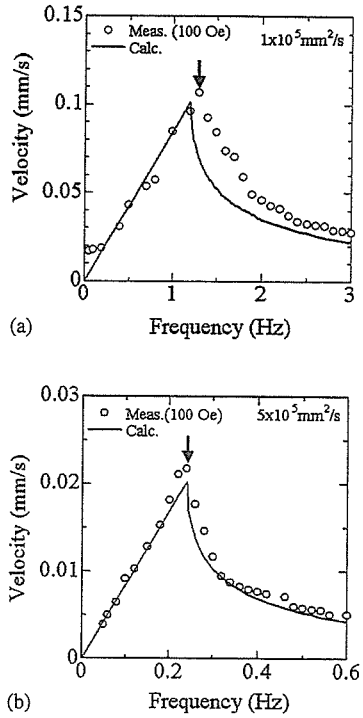

Fig. 7. Relation between frequency and swimming velocity of the micro-machine: (a) $\nu = 1 \times 10^5$ mm^2/s; (b) $\nu = 5 \times 10^5$ mm^2/s.

Fig. 8 shows the relation between the frequency and the drag. The viscous shear stress generated on the micro-machine body is set to shear (cylinder). The viscous shear stress generated on the spiral-blade is set to shear (blade). The pressure difference between front and back of the ends of the micro-machine is set to pressure (disk). All parameters added together are set as the total. As a result of analysis, all parameters increase in proportion to the frequency. The ends of the micro-machine produce only a small effect, while the viscous stress generated on the micro-machine surface produces a large effect, we cannot discuss whether the calculate values of drag are exact or not. However, the drag is the calculated force of axial direction of the micro-machine. Since the result of that swimming velocity of the micro-machine is good agreement as already shown in Fig. 7, the value of drag is exact.

Fig. 9 shows the relation between the frequency and the load torque. In addition to shear (blade) and shear (cylinder), the pressure difference between front and back of the spiral blade is set to pressure (blade). The viscous shear stress generated on the ends of the micro-machine is set to shear (disk). As a result of analysis, all of the parameters increase in proportion to the frequency. It is found that the shear is much lager than pressure. Since shear is based on the viscous force and pressure is based on the inertial force, the result indicates the viscous force is much dominant than the inertial force. The Reynolds number is expressed with the

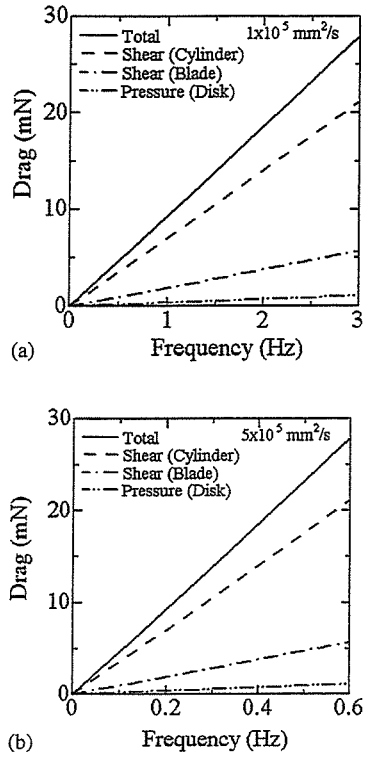

Fig. 8. Relation between frequency and drag: (a) $\nu = 1 \times 10^5$ mm^2/s; (b) $\nu = 5 \times 10^5$ mm^2/s.

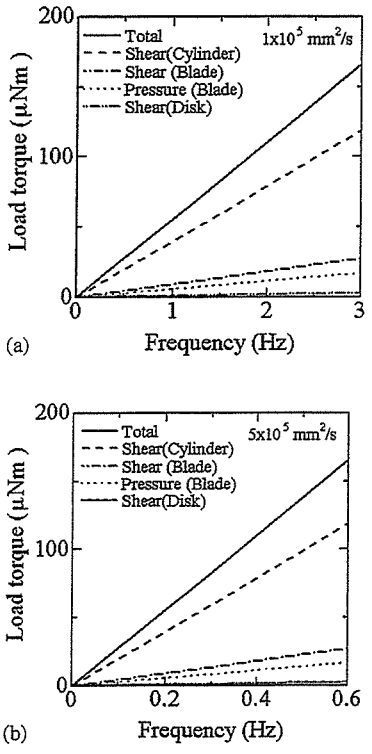

Fig. 9. Relation between frequency and load torque: (a) $\nu = 1 \times 10^5$ mm^2/s; (b) $\nu = 5 \times 10^5$ mm^2/s.

Table 2
Load torque of the step-out frequency

Kinematic viscosity ν (mm^2/s)	Analytical result (μm)	Experimental result(μm)
1×10^5	72	66
5×10^5	66	66

ratio of the viscous force and the inertial force. When the viscous force is larger, the Reynolds number becomes lower. Therefore, this result shows this analysis is suitable for a low Reynolds number condition.

The value of load torque cannot obtain from the experiment as well as the value of drag. However, the value of load torque is confirmed by measuring the step-out frequency. At the step-out frequency, the load torque equals to the applied magnetic torque. Therefore, we can estimate the load torque at the step-out frequency as the maximum magnetic torque. Table 2 shows the analytical and experimental load torque in two kinds of liquid. As the valued are in good agreement, the analysis can explain the experimental result.

As our experimental results mostly agreed with the results obtained from our 3D analysis, we could establish the reliability of our 3D method for the analysis of the swimming properties of the micro-machine.

3. Summary

We theoretically analyzed the swimming properties of a spiral-type magnetic micro-machine using the 3D finite volume method. This analytical method was able to solve the velocity and the pressure distribution of the micro-machine circumference. Using our analysis results, we solved the velocity of micro-machine, thrust, drag, and load torque. In addition, we attempted to solve equations to show the effects of the micro-machine rotation direction on the swimming velocity after step-out frequency. Consequently, the calculation and experimental value of the swimming velocity were in agreement before and after step-out frequency. The Frequency calculated from the load torque and magnetic torque was also agreed well with the step-out frequency determined in the experiment.

Therefore, the method for 3D analysis to a low Reynolds number without fitting parameter was established. The micro-machine can be designed without experiment by using the 3D analysis method.

References

[1] M. Sendoh, N. Ajiro, K. Ishiyama, M. Inoue, K.I. Arai, Effect of machine shape on swimming properties of the spiral-type magnetic micro-machine, IEEE Trans. Magn. 36 (1999) 3688–3690.

[2] M. Sendoh, A. Yamazaki, K. Ishiyama, M. Inoue, T. Hayase, K.I. Arai, Swimming of spiral-type magnetic micro-machine under very low reynolds number condition, J. Mag. Soc. Jan. 25 (2001) 1223–1226 (in Japanese).

[3] T. Hayase, J.A.C. Humphrey, R. Greif, Numerical calculation of convective heat transfer between rotating coaxial cylinders with periodically embedded cavities, J. Heat Trans. 114 (1992) 589–597.
[4] Douglas John Goering, The Influence of Curvature and Buoyancy in Three-Dimensional Pipe Flows, Ph.D. Dissertation at the University of California, Berkeley, 1989.
[5] S.V. Patankar, Numerical Heat Transfer and Fluid Flow, Hemisphere, 1980.
[6] T. Hayase, J.A.C. Humphrey, R. Greif, A consistently formulated QUICK scheme for fast and stable convergence using finite-volume iterative calculation procedures, J. Comput. Phys. 98-1 (1992) 108–118.
[7] T. Kambe, Fluid Dynamics, Shokabo, Tokyo, 1995.
[8] M. Sendoh, K. Ishiyama, M. Yamaguchi, K.I. Arai, Starting characteristics of spiral-type magnetic micro-machine, J. Mag. Soc. Jan. 26 (2002) 653–656 (in Japanese).

Biographies

A. Yamazaki received a BS degree in Mechanical Engineering from the Science University of Tokyo, Japan, in 1998, and a MS degree in Electrical Engineering from Tohoku University, Japan, in 2002. She is currently enrolled in the doctorate course at Tohoku University. Her research interests are in the area of magnetic actuators.

M. Sendoh received his MS degree in Electrical Engineering from Tohoku University, Japan, in 2000. He is currently enrolled in the doctorate course at Tohoku University. His research interests are in the area of magnetic actuators.

K. Ishiyama received his MS and PhD degree in Electrical Engineering from Tohoku University, Japan, in 1986 and 1993, respectively. He is currently working as a research associate at the Research Institute of Electrical Communication, Tohoku University. His research interests are in the area of magnetic actuators and magnetic materials.

T. Hayase received his MS and PhD degrees in Mechanical Engineering from Nagoya University, Japan, in 1980 and 1987, respectively. He is currently working as a professor at the Institute of Fluid Science, Tohoku University. His research interests are in the area of computational fluid dynamics and bio-fluid informatics.

K.I. Arai received his MS and PhD degree in Electrical Engineering from Tohoku University, Japan, in 1968 and 1971, respectively. He is currently working as a professor at the Research Institute of Electrical Communication, Tohoku University. His research interests are in the areas of physical properties and applications of magnetic materials.

Magnetic micromachines prepared by ferrite plating technique

K. Nishimura,[a] H. Uchida, and M. Inoue
Department of Electrical and Electronic Engineering, Toyohashi University of Technology, Toyohashi 441-8580, Japan

M. Sendoh, K. Ishiyama, and K. I. Arai
Research Institute of Electrical Communication, Tohoku University, Sendai, 980-8577, Japan

(Presented on 12 November 2002)

By the sterolithography technique and the ferrite plating, we fabricated three types of magnetic micromachines which coated Fe_3O_4, $Co_{0.39}Fe_{2.61}O_4$, and $Co_{0.45}Fe_{2.55}O_4$, respectively. The stereolithography technique enables one to form the spiral-shape resinous templates and the ferrite plating enables one to coat the ferrites uniformly onto these templates from an aqueous solution. The total machine weight is light because a resin of the template body is almost the same density as water. We verified that the machines swim freely and wirelessly in water by applying a rotational magnetic field. As these machines coated with ferrites have the biocompatibility, there is the possibility of medical microrobots which swim in the human body for medical operations. © *2003 American Institute of Physics.* [DOI: 10.1063/1.1556928]

I. INTRODUCTION

Spiral-shaped magnetic micromachines driven by a magnetic field have attracted a great deal of attention in the medical field.[1] As they swim freely and wirelessly in the human body, they can perform a cancer operation, blood clot operation, and so on. To develop such medical micromachines, they should fulfill the following requirements simultaneously: First, their size needs to be in submillimeter scale so as to introduce the machines into blood vessels, body fluids, intestinal fluids, and so on. Second, we have to choose appropriate constitutive materials which have biocompatibility and chemical stability in the human body. Third, their density needs to be as small as that of blood. We propose the magnetic micromachines meet all the above requirements. They are completely solid-state machines coated ferrites onto the resinous templates. We fabricated these micromachine using the stereolithography technique[2] and ferrite plating.[3]

II. EXPERIMENT

The template body used the spiral-shaped resinous substrate prepared by stereolithography technique. It has a diameter of 1.2 mm, a length of 15 mm, and a spiral submillimeter blade. As shown in Table I, we plated ferrites of three types on the templates: magnetite (A type), Co solid solution ferrite using only metal (II) ions (B type), and Co solid solution ferrite using Fe^{3+} ions (C type). These reaction solutions and an oxidizing solution of oxidizing reagent ($NaNO_2$ of 0.01 mol/l)[3] $+p$H buffer (CH_3COONH_4 of 1.0 mol/l) were simultaneously conducted into the vessel at the same flow rate of 3 cm^3/min as shown in Fig. 1. By applying ultrasound waves (19.5 kHz, 600 W) to a reaction solution into the vessel, the temperature increased and the solution was mixed. The whole temperature and the pH value were at 90 °C and at pH = 6.0. The pH value of the mixture solution was measured frequently from the part of fresh drain. The plating times ranged from 5 to 8 h.

The samples were subjected to x-ray diffraction (XRD) analyses using Cu $K\alpha$ radiation. The chemical compositions of the coating samples were determined by energy dispersion x-ray analysis (EDX). For measurements of XRD and EDX, we used samples which plated onto glass substrates at the same time that we plated on resinous substrates. We directly measured magnetic properties for micromachines coated with ferrites using a vibrating sample magnetometer.

III. RESULTS AND DISCUSSIONS

The micromachine coated with Fe_3O_4, performed for 533 min. As shown in Fig. 2(A), the Fe_3O_4 coating micromachine has the softest coercivity of 60 Oe and the highest magnetization of 0.181 emu at 10 kOe of three samples. For the micromachine coated with the ferrite of B type, we plated for 300 min. The concentration of the ferrite of B type was $Co_{0.39}Fe_{2.61}O_4$ by EDX analysis. This magnetization curve was shown in Fig. 2(B). The coercivity and the magnetization are 860 Oe and 0.080 emu at 10 kOe, respectively. For the micromachine of C type, we coated for 333 min. The concentration of the ferrite of C type was $Co_{0.45}Fe_{2.55}O_4$. This increased the solubility of Co^{2+} ions than the former. We confirmed an increase of the solubility of other metal (II)

TABLE I. Reaction solutions of three types of machines.

Type of machine	Reaction solution (mol/l)		
	$FeCl_2$	$CoCl_3$	$FeCl_3$
A	0.1	0	0
B	0.075	0.025	0
C	0.072	0.025	0.003

[a]Author to whom correspondence should be addressed; electronic mail: nishimura@eee.tut.ac.jp

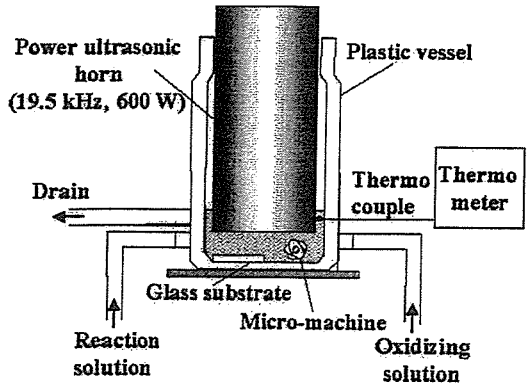

FIG. 1. Apparatus of ultrasound enhanced ferrite plating.

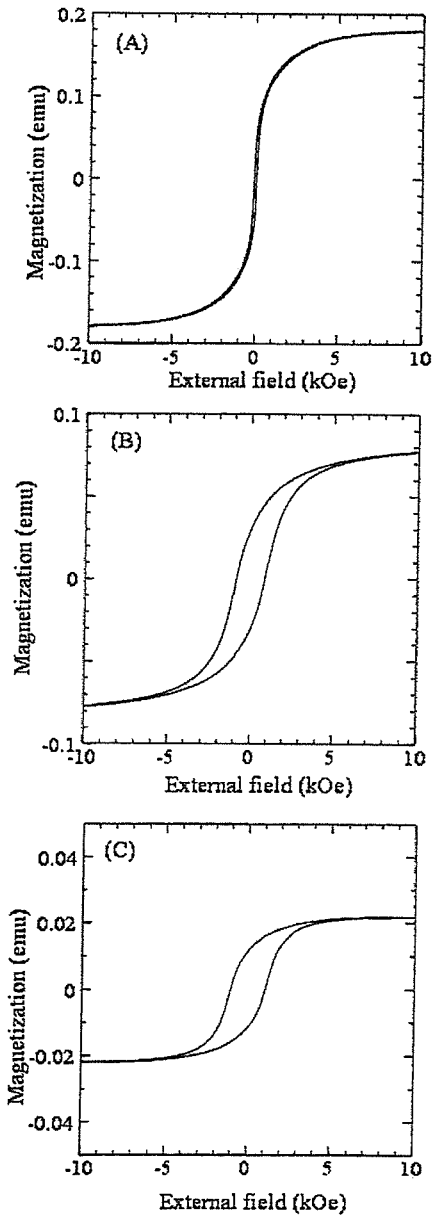

FIG. 2. Magnetization curves for machines plated (A) Fe_3O_4, (B) $Co_{0.39}Fe_{2.61}O_4$, and (C) $Co_{0.45}Fe_{2.55}O_4$.

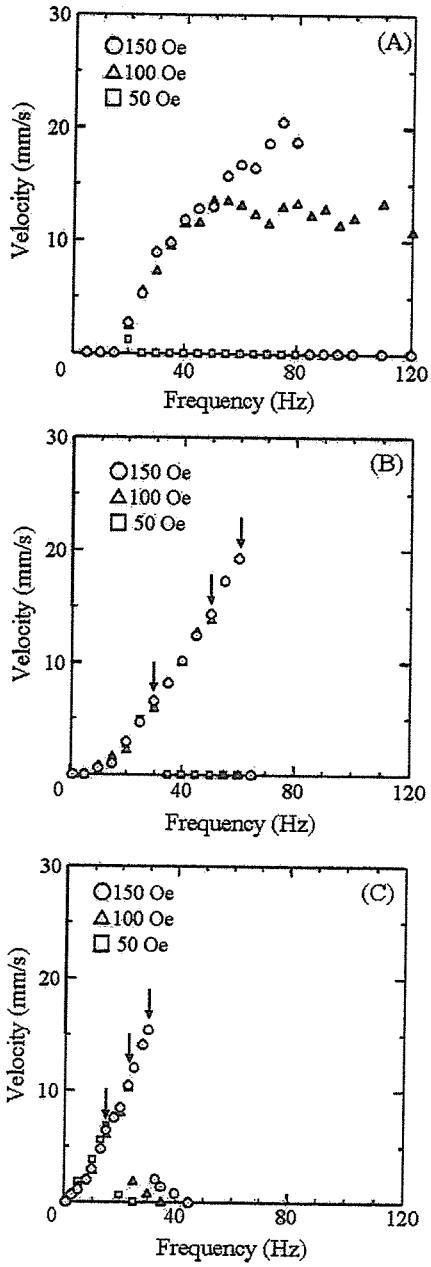

FIG. 3. Swimming velocity of machines plated (A) Fe_3O_4, (B) $Co_{0.39}Fe_{2.61}O_4$, and (C) $Co_{0.45}Fe_{2.55}O_4$, which are plotted as a function of frequency.

ions by adding Fe^{3+} ions by the previous study.[4] In this study, the similar effect is considered. As shown in Fig. 2(C), we obtained the coercivity of 1060 Oe, and the magnetization of 0.022 emu at 10 kOe. The coercivity was the biggest of the three micromachines. The magnetization is the smallest of them. All samples have isotropic magnetic properties and have spinel structure as revealed by XRD.

After we magnetized the samples perpendicularly to the direction of length, these light micromachines swim in water by applying a rotational magnetic field. Figure 3 shows the quantitative relation between swimming velocity and rotation frequency of field: the micromachine of A type shown in Fig. 3(A) swims at rotation magnetic field intensity of more than 100 Oe and at rotation frequency of more than 20 Hz.

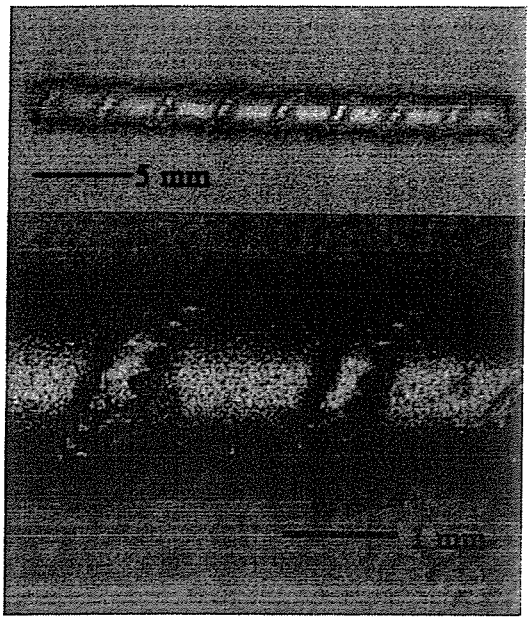

FIG. 4. Typical photos of magnetic micromachine coated with $Co_{0.39}Fe_{2.61}O_4$.

As this micromachine is magnetized by the rotation magnetization at over coercivity of 60 Oe, this micromachine swims by inducing with the rotation frequency. In the case of Co solid solution ferrites having large coercivity [Figs. 3(B) and 3(C)], the swimming velocity increased in proportion to the rotational frequency, and stepped out at a certain frequency whose value becomes higher as the field intensity increases. They swim by synchronizing the residual magnetization with the rotation frequency.

As shown in Fig. 4, all coating samples were plated uniformly onto a tiny template with spiral structure.

IV. CONCLUDING REMARKS

We succeeded in coating the three types of ferrites uniformly onto a resinous substrate with spiral structure prepared by stereolithography. Ferrites are Fe_3O_4 made from only Fe^{2+} ions, $Co_{0.39}Fe_{2.61}O_4$ made from $Fe^{2+}+Co^{2+}$ ions, and $Co_{0.45}Fe_{2.55}O_4$ made from $Fe^{2+}+Co^{2+}+Fe^{3+}$ ions, respectively. By adding the Fe^{3+} ions slightly, the solubility of Co^{2+} ions increased and the coercivity became large from 860 to 1060 Oe. Into water, the micromachines coated with ferrites were able to swim by applying a rotational magnetic field. They are a solid-state wireless micromachine. As magnetite coated machines have the biocompatibility and small density, we expect the possibility of new medical operation.

[1] For example, K. Ishiyama, M. Sendoh, A. Yamazaki, and K. I. Arai, Sens. Actuators **91**, 141 (2001).
[2] S. Maruo and K. Ikuta, Appl. Phys. Lett. **76**, 2656 (2000).
[3] M. Abe, T. Itoh, and Y. Tamaura, Thin Solid Films **216**, 155 (1992).
[4] K. Nishimura, M. Abe, and M. Inoue, IEEE Trans. Magn. **38**, 1 (2002).

Available online at www.sciencedirect.com
SCIENCE DIRECT®
ELSEVIER
Journal of Magnetism and Magnetic Materials 272–276 (2004) e1741–e1742
journal of magnetism and magnetic materials
www.elsevier.com/locate/jmmm

Wireless micro swimming machine with magnetic thin film

Aya Yamazaki[a,*], Masahiko Sendoh[a], Kazushi Ishiyama[a], Ken Ichi Arai[a], Ryutaro Kato[b], Masaki Nakano[b], Hirotoshi Fukunaga[b]

[a] *Research Institute of Electrical Communication, Tohoku University, 2-1-1 Katahira Aoba-ku, Sendai 980-8577, Japan*
[b] *Nagasaki University, 1-14 Bunkyo-machi, Nagasaki 852-8521, Japan*

Abstract

As the magnetic micro-machines are driven by a magnetic field, they require no power supply cables, no batteries, and no controlling systems on the machine body. We fabricated the spiral-type micro-machine (outer diameter; 0.14 mm, length; 1.0 mm) by a tungsten wire (ϕ 20 μm). NdFeB film magnet was deposited on the spiral-machine by the PLD method. In the experiment, the wireless micro-machine swam at the speed of 0.2–1.6 mm/s. This result indicated that the spiral shape was suitable for miniature swimming machine.

PACS: 85.70.Yv; 85.70.Rp

Keywords: Spiral structure; Magnetic micro-machine; Magnetic thin film; Rotating magnetic field; Reynolds number

1. Introduction

Magnetic micro-machines are driven by a magnetic field. They require no power supply cables, no batteries, and no controlling systems on the machine body. In previous studies, we examined the swimming properties of a spiral-type magnetic micro-machine (outer diameter of 1.5 or 0.8 mm) with the bulk magnet [1,2]. We found that the spiral structure was applicable to swim under a very wide range of Reynolds numbers ($10^{-7} < Re < 10^{3}$), and that the spiral structure was suitable for the miniaturization. However, it is difficult to reduce the size using the bulk magnet. Therefore, we attempted the miniaturization of the micro-machine with magnetic thin film.

2. Magnetic micro-machine

Fig. 1 shows a photograph of the spiral-type magnetic micro-machine. The micro-machine was fabricated with a tungsten wire of a diameter 20 μm. The size of micro-machine has the outer diameter of 0.14 mm and length of 1.0 mm. On the micro-machine, NdFeB film magnet was deposited by the PLD method and thickness of a film was several micros [3]. As the magnet was magnetized in the diameter direction, the machine rotated in synch with the rotating external magnetic field and the spiral structure was generated propellant force.

3. Experiment and analysis result

3.1. Swimming velocity

The spiral-type magnetic micro-machine with thin wire and thin film magnet could swim by the rotating external magnetic field. Fig. 2 shows the relation between the frequency and the swimming velocity of the micro-machine. We used three types of liquids with kinematic viscosity (1, 10, 100 mm^2/s). In Fig. 2, the plots show the experimental results, and the solid line shows the analysis result [4]. The arrow in this graph was the step-out frequency at kinematic viscosity of 100 mm^2/s. At the step-out frequency, the rotation of

*Corresponding author. Tel.: +81-22-217-5488; fax: +81-22-217-5728.
E-mail address: aya@riec.tohoku.ac.jp (A. Yamazaki).

0304-8853/$ - see front matter © 2003 Elsevier B.V. All rights reserved.
doi:10.1016/j.jmmm.2003.12.337

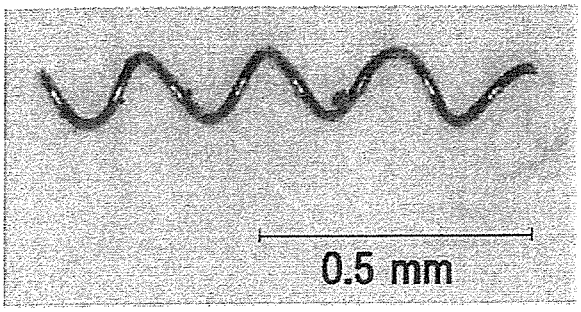

Fig. 1. Photograph of the spiral-type magnetic micro-machine.

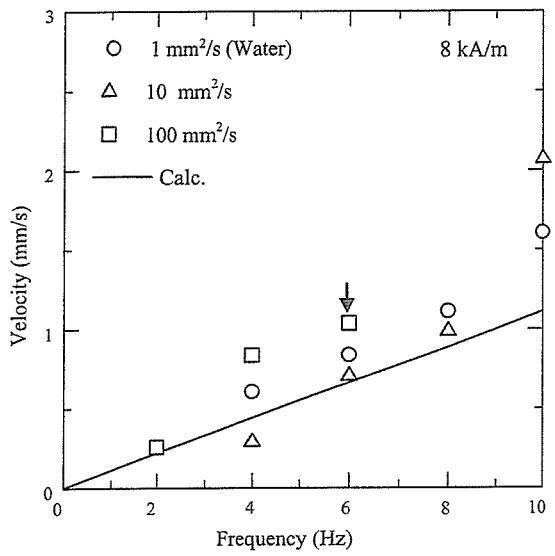

Fig. 2. Relation between frequency and swimming velocity of experimental and analysis.

the machine could not be synchronized to the rotational magnetic field. The micro-machine swam at the speed of 0.2–1.6 mm/s. The Reynolds numbers on this condition were 2×10^{-3}–1.6. This result shows that the spiral shape is suitable for miniature swimming machine.

3.2. Load torque

The value of load torque which the micro-machine receives from the fluid is difficult to obtain by the experiment. However the value of load torque is confirmed by measuring the step-out frequency. At the step-out frequency, the load torque equals to the applied magnetic torque. Therefore, the minimum magnetic field which the micro-machine can rotate was measured at the frequency of the magnetic field of 10 Hz. From this result, the applied magnetic torque was estimated.

Fig. 3 shows the relation between the kinematic viscosity and the torque. The plots show the experimental results of the magnetic torque and the solid line shows the analysis result of load torque [4]. The torque increased with the increase in the kinematic viscosity. In the experiment of swimming velocity, as the magnetic field was 8 kA/m, the step-out frequency was not seen by 1 and 10 mm^2/s. In order for the micro-machine to swim, the required magnetic torque is estimated as 10^{-3}–1 nNm and the magnetic field is 0.1–10 kA/m. Therefore, the magnetic torque was very small and the thickness of a magnetic film is realizable by several microns.

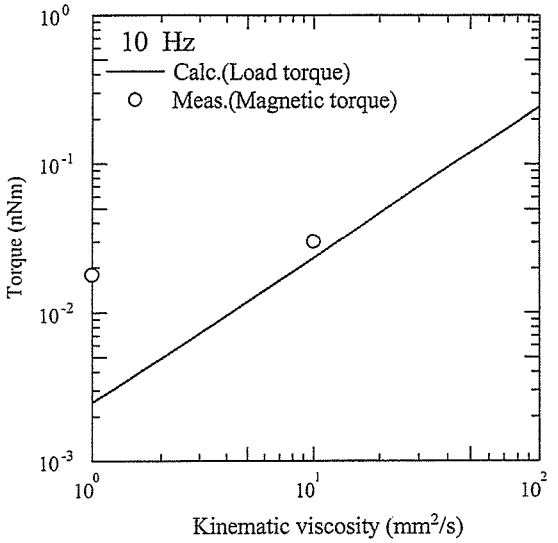

Fig. 3. Relation between kinematic viscosity of liquid and torque.

4. Summary

We fabricated the magnetic micro-machine that was composed of spiral-shaped thin wire and the thin film magnet. The micro-machine with outer diameter 0.14 mm was able to swim wirelessly in the liquids. This result indicated that the spiral shape was suitable for miniature swimming machine. The magnetic torque required for the drive of spiral-type micro-machine was very small, and it was shown that the value could be realized with a magnetic thin film.

References

[1] K. Ishiyama, et al., Sensors and Actuators A 91 (2001) 141.
[2] A. Yamazaki, et al., J. Magn. Soc. Jpn. 27 (2002) 645.
[3] M. Nakano, et al., IEEE Trans, Magn. 38 (2002) 2913.
[4] M. Sendoh, et al., J. Robot. Mec. 12 (2000) 165.

日本応用磁気学会誌 28, 632–635 (2004)

〈論 文〉

らせん型磁気マイクロマシンの泳動特性に対するらせん長の影響

Effect of Machine Length on Swimming Properties of Spiral Magnetic Micro-Machine

山崎彩・仙道雅彦・石山和志・荒井賢一

東北大学電気通信研究所，仙台市青葉区片平 2-1-1（〒980-8577）

A. Yamazaki, M. Sendoh, K. Ishiyama and K. I. Arai

Research Institute of Electrical Communication, Tohoku University, *2-1-1 Katahira Aoba-ku Sendai 980-8577*

In previous studies, we examined a magnetic micro-machine composed a magnet and spiral structure. As the magnet was magnetized in the diameter direction, the micro-machine rotated in synchronism with the rotating magnetic field. This time, we fabricated two types of spiral magnetic micro-machines. One had the magnet and the wire of the spiral structure (head type). The other had the wire of the spiral structure (spiral type). We examined the influence of the micro-machine length. As a result, we found that the swimming velocity of the head type micro-machine depended on the machine length. The swimming velocity of the spiral type micro-machine does not depend on the machine length.

Key words: micro-machine, spiral blade, rotating magnetic field, swimming velocity, machine length

1. はじめに

著者らは，Fig. 1 に示すらせん形状に加工したワイヤと磁石から構成される磁気マイクロマシンを開発した [1) 2)]．この磁気マイクロマシンは，搭載している磁石が半径方向に着磁されているため，外部から印加される回転磁界に同期して回転する．この磁石の回転がらせん部分で推力に変換され，磁気マイクロマシンは推進する．従って，磁気マイクロマシンは，電源を搭載せず，ワイヤレスでエネルギー供給が可能である．磁気マイクロマシンは，回転磁界面に垂直な姿勢を保ちながら推進を行う．従って，回転磁界面の方向を制御することで，磁気マイクロマシンの推進方向制御をワイヤレスで行うことが可能となる [3)]．

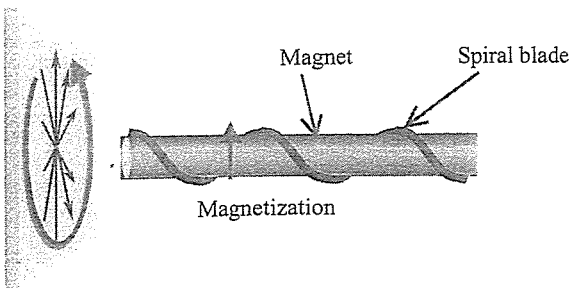

Fig. 1 Schematic view of magnetic micro-machine.

らせん型マイクロマシンの形状を決める要素として，マシンの直径，マシンの長さ，らせん形状がある．これらの要素が泳動特性に与える影響を検討し，駆動に必要な磁気トルク，効率の良い形状について検討し，マシン設計を行う必要がある．我々は先の研究において，有限体積法を用いた流体力学的泳動特性解析手法を確立し，マシン直径が 0.15～1.5 mm の磁気マイクロマシンについて，実験と解析から泳動特性の検討を行った．その結果，らせん構造の磁気マイクロマシンは，レイノルズ数が 10^{-7}～10^{3} と幅広い条件下で駆動することができ，らせん構造が小形化に適した構造であることを示してきた [4) 5)]．らせんの高さ，角度の変化による泳動特性への影響について検討を行い，らせん形状に関する設計指針が得られた [5) 6)]．

本研究では，これまでに検討を行っていないマシンの長さによる泳動特性の影響について実験と解析から検討を行った．解析には，先の研究で確立した有限体積法を用いた 3 次元泳動特性解析手法 [7)] を用いて行った．

2. 磁気マイクロマシン

Fig. 2 (a)，Fig. 2 (b) に検討を行った 2 種類の磁気マイクロマシンの写真を示す．Fig. 2 (a)のマシンは，半径方向に着磁された SmFeN 磁石(ϕ 1.2×0.55 mm)とらせん形状に加工した直径 0.15 mm のタングステンワイヤから構成されており，以後 Head 型マイクロマシンと呼ぶ．このマシンのらせんピッチは 4.4 mm である．Fig. 2 (b)は，直径 20 μm のタングステンワイヤをらせんピッチ 0.2 mm で加工したマシン(Spiral 型マイクロマシン)である．ワイヤ表面に PLD (Pulsed Laser Deposition) 法 [8)] を用いて，NdFeB 薄膜磁石を数μm 積層した．磁化方向は半径方向である．

3. 実験と解析結果

3.1 Head 型マイクロマシン

Head 型マイクロマシンの実験では，動粘度 1×10^{4} mm²/s のシリコーンオイルで満たされた試験管内にマシンを挿入した．外部から 12 kA/m (150 Oe)の回転磁界を印